journal

J. Am. Ceram. Soc., 79 [8] 2127-33 (1996)

Cracking of Laminates Subjected to Biaxial Tensile Stresses

Craig Hillman,[*] Zhigang Suo, and Fred F. Lange[*]

Materials Department, University of California, Santa Barbara, Santa Barbara, California 93106

During the processing of laminar ceramic, biaxial residual stresses can arise due to differential thermal contraction between unlike layers. A tensile stress can cause preexisting flaws to extend across the layer and into the adjacent layers and then tunnel until they meet either another crack or a free surface. A previous analysis has shown that for a given residual stress there is a critical layer thickness, below which no tunnel cracks will exist, regardless of initial flaw size. Here, the previous analysis was modified to take into account the crack extension into adjacent layers. To determine the validity of the analysis, laminates composed of alternating layers of zirconia and alumina/zirconia were fabricated by a sequential centrifugation technique. The composition of the alumina/zirconia layer was varied to change the biaxial, tensile stresses in the zirconia layer. Observations were then made to determine the critical layer thickness for tunnel cracks and their extension into the adjacent layers. These observations were compared to the theoretical predictions.

I. Introduction

LAYERED ceramics play important roles in modern life. They have been used in the electronics industry as multilayer substrates,[1] capacitors,[2] and fuel–air sensors.[3] Ceramic laminates are being considered for structural applications[4–9] to impart damage tolerance for conditions where cracks extend at constant strains. The analysis and observations reported here also apply to two materials that are bonded together by a layer of a third material, as either an adhesive[10,11] or a braze.[12]

During processing, residual stresses arise due to differential strains developed during drying, pyrolysis of binders, densification, and contraction during cooling. If the residual tensile stress in a layer is large enough, it will cause preexisting flaws to "tunnel" in the layer, until it meets a free surface (either the surface of the laminate or another tunnel crack). Under biaxial tension, multiple tunnel cracks produce a mud crack pattern, similar to those seen in thin films[13] and brittle adhesive layers.[10,11]

Ho and Suo[14] developed a strain energy release rate expression for the tunnel crack in layers subjected to biaxial tension. For a given residual stress, a critical layer thickness exists below which no tunnel cracks will exist, regardless of the initial flaw size. Consequently, crack-free ceramic laminates can be processed with a high reliability. Similar steady-state cracking in thin films was previously reported by Hu and Evans.[15]

The purpose of this paper is to experimentally verify Ho and Suo's theoretical predictions. In this experiment, a thin zirconia layer was sandwiched between two thicker layers of an alumina/zirconia composite. The laminate was densified at high temperature. Zirconia has a larger coefficient of thermal expansion (CTE) than alumina. As shown in Fig. 1, if the layers were separated, the zirconia layer would contract more than the alumina/zirconia layers during cooling. The difference in the strains is given by

$$\varepsilon_r = \int_{T_i}^{T_f} (\alpha_{Zr} - \alpha_{Al/Zr})\,dT \tag{1}$$

where T_i and T_f are the initial and final temperatures during cooling, and α_{Zr} and $\alpha_{Al/Zr}$ are the CTE's of the zirconia layer and the alumina/zirconia layers, respectively. By varying the composition of the bulk alumina/zirconia layer, and thus varying $\alpha_{Al/Zr}$, the residual strain was changed in the thinner zirconia layers. If the layers are bonded, the misfit strain (Eq. (1)) induces a residual tensile stress in the zirconia layer.[14]

$$\sigma_r = \frac{\varepsilon_r E_{Zr}}{1 - \nu_{Zr}}\left[1 + \frac{t}{w}\frac{E_{Zr}/(1 - \nu_{Zr})}{E_{Al/Zr}/(1 - \nu_{Al/Zr})}\right]^{-1} \tag{2}$$

Here t and w are the thicknesses of the zirconia and the alumina/zirconia layers, and E and ν are Young's modulus and Poisson's

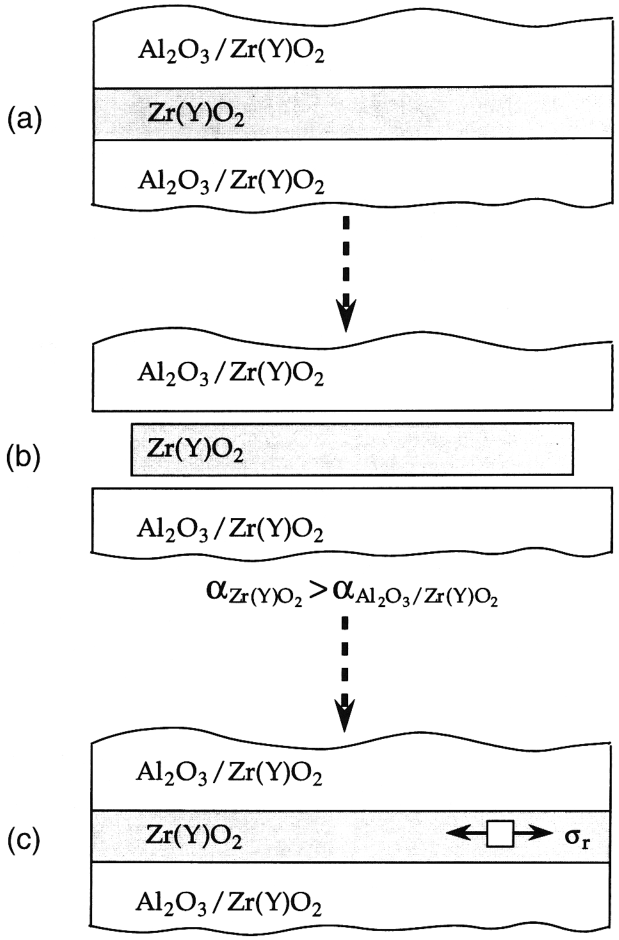

Fig. 1. (a) An embedded layer of $Zr(Y)O_2$ sandwiched between two bulk layers of $Al_2O_3/Zr(Y)O_2$. (b) During cooling from processing temperatures, the $Zr(Y)O_2$ layer would shrink more due to its higher coefficient of thermal expansion, α. (c) Due to strong interfaces, the $Zr(Y)O_2$ layer is constrained from shrinking, producing a biaxial, residual tensile stress in the embedded layer.

D. J. Green—contributing editor

Manuscript No. 192540. Received June 15, 1995; approved November 6, 1995.
Supported by the Office of Naval Research under Contract No. N00014-90-J-1441.

[*] Member, American Ceramic Society.

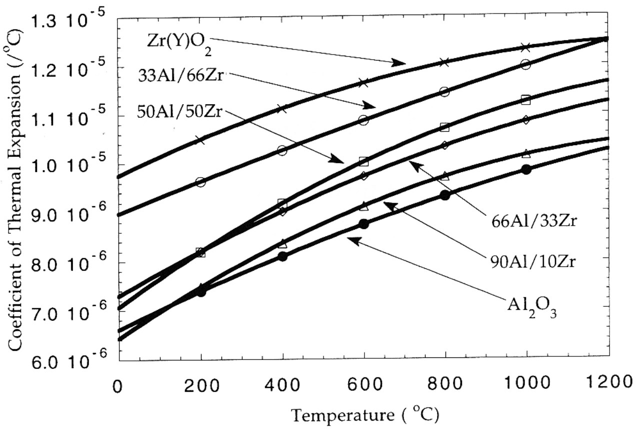

Fig. 2. Plot of coefficient of thermal expansion (CTE) vs temperature (0°C–1000°C) for $Zr(Y)O_2$ and various compositions of $Al_2O_3/Zr(Y)O_2$.

Table I. Average Coefficient of Thermal Expansion (20°–1000°C)(10^{-6}/K)

	Average CTE		
	Harrop	Rockwell	Theory[21]
$Zr(Y)O_2$	11.30	11.4	N/A
0.33Al/0.66Zr	10.56	N/A	10.05
0.5Al/0.5Zr	9.51	9.5	9.66
0.66Al/0.33Zr	9.31	N/A	9.11
0.9Al/0.1Zr	8.64	N/A	8.62
Al_2O_3	8.39[†]	N/A	N/A

[†] The coefficient of thermal expansion for alumina was taken from Ref. 33.

ratio of the two layers. If the zirconia layer is much thinner than the alumina/zirconia composite, $t/w \ll 1$, the stress in the zirconia layer becomes

$$\sigma_r = \frac{\varepsilon_r E_{Zr}}{1 - \nu_{Zr}} \tag{3}$$

and the stress in the alumina/zirconia layers is reduced to zero.

II. Experimental Method

The laminates consisted of thin layers of either tetragonal-$Zr(3Y)O_2$ or cubic-$Zr(8Y)O_2$[†] (thicknesses between 10 and 500 μm) sandwiched between thick layers of $Al_2O_3/Zr(Y)O_2$- (≈3000 μm). Several $Al_2O_3/Zr(Y)O_2$ compositions were used to vary the residual stress in the zirconia layer. The laminates were fabricated by a sequential centrifugation method described elsewhere.[6,16] The method uses a new colloidal processing technique,[17,18] where a short-range repulsive potential is produced by adding salt (e.g., NH_4Cl) to a dispersed, aqueous slurry. The short-range repulsive potential produces a weakly attractive particle network that allows particles to pack to a high relative density by either pressure filtration[17,18] or centrifugation[19] and prevents mass segregation during centrifugation.[20]

A dispersed, aqueous slurry containing 0.005 volume fraction of $Zr(Y)O_2$ powder ($Zr(Y)O_2$ powder: TZ-3Y, TZ-8Y, Tosoh, Tokyo, Japan) was prepared at pH 2; 1.0*M* of NH_4Cl was then added to create a weakly attractive network. This slurry was used to produce thin $Zr(Y)O_2$ layers. In a similar manner, a second slurry was prepared containing 0.10 volume fraction of $Zr(Y)O_2$ and Al_2O_3 (Al_2O_3 powder: AKP-50, Sumitomo Chemical, New York) powders (0.50 volume fraction each) was used to produce thick $Al_2O_3/Zr(Y)O_2$ layers. A volume V of the appropriate slurry containing the volume fraction of powder, ϕ, was poured into the centrifuge tube, of area A, to form a layer of thickness

$$t = \frac{V\phi}{A}$$

By changing either the volume fraction of powder in the slurry or the volume poured into the tube, one could vary the layer thickness formed during centrifugation. For the current study, the predetermined volume of the $Al_2O_3/Zr(Y)O_2$ slurry was poured into a 50 mL centrifuge tube (50 mL polyethylene centrifuge tubes, Nalgene) and centrifuged at 3200 rpm (centripetal acceleration ~ 1900 g) for 2 h (optimum time for maximum particle packing density determined in Ref. 20). The tubes were accelerated slowly up to the highest speed in order to ensure a smooth surface and a uniform layer thickness. After forming one thick $Al_2O_3/Zr(Y)O_2$ layer, the clear supernatant was poured off and a predetermined volume of the $Zr(Y)O_2$ slurry was introduced into the tube to form a thin $Zr(Y)O_2$ layer by centrifugation. This process was repeated until the desired number of thin $Zr(Y)O_2$ layers were formed, each with a different thickness, sandwiched between much thicker $Al_2O_3/Zr(Y)O_2$ layers.

The laminates were air-dried and then heated at 2°C/min to 1500°C for 1 h to produce dense, laminar specimens. The laminates were sectioned by diamond cutting, polished, and then examined with a scanning electron microscope for cracks (SEM) (840 SEM, JEOL, Tokyo, Japan). The layer thickness for which no cracks were observed was determined to be the critical layer thickness.

Bodies of all the compositions used to form laminates were also consolidated to make specimens to measure coefficients of thermal expansion, which were used to determine the residual stress in the $Zr(Y)O_2$ layer. CTE measurements were made courtesy of both Harrop Industries (Columbus, OH) and Rockwell International Science Center to temperatures of 1500°C. Theoretical values of the CTE were also calculated[21] for the different alumina/zirconia compositions using the measured CTE's for the two end members and their elastic properties.

The fracture toughness of the embedded zirconia layers was determined using the single-edge-precracked-beam (SEPB) method.[22] Rectangular beam specimens (3 mm × 4 mm × 30 mm) were used. Three indents were used to introduce small cracks in the center of the tensile face (30 kg loads for t-$Zr(3Y)O_2$; 10 kg loads for c-$Zr(8Y)O_2$). A precrack was "popped-in" using the bridge-indentation apparatus described in Ref. 22. Once the precrack met the conditions of ASTM E399 8.2 (parallel to the thickness direction, equilength on both sides of the beam), its length was measured, and the beam was loaded to failure in four-point bend. K_{Ic} was calculated using the K function reported by Srawley.[23]

Table II. Material Properties

	α (10^{-6}/K) 25°–1500°C	E(GPa)	ν	K_{Ic} (MPa·m$^{1/2}$)
$Zr(Y)O_2$	$9.75 \times 10^{-6} + (4.00 \times 10^{-9})T - (1.44 \times 10^{-12})T^2$	205 (Ref. 30)	0.32 (Ref. 36)	6.2[†], 2.1[‡]
0.33Al/0.66Zr	$8.97 \times 10^{-6} + (3.38 \times 10^{-9})T - (3.90 \times 10^{-13})T^2$	260[§]	0.32	
0.5Al/0.5Zr	$7.06 \times 10^{-6} + (7.80 \times 10^{-9})T - (5.83 \times 10^{-12})T^2$	300 (Refs. 30, 34)	0.32 (Ref. 36)	
0.66Al/0.33Zr	$7.29 \times 10^{-6} + (4.28 \times 10^{-9})T - (1.28 \times 10^{-12})T^2$	320[§]	0.32	
0.9Al/0.1Zr	$6.42 \times 10^{-6} + (5.64 \times 10^{-9})T - (1.92 \times 10^{-12})T^2$	360[§]	0.32	
Al_2O_3	$6.6 \times 10^{-6} + (4.1 \times 10^{-9})T - (8.9 \times 10^{-13})T^2$ (Ref. 31)	380 (Ref. 35)	0.32 (Ref. 37)	

[†] Value for t-$Zr(3Y)O_2$. [‡] Value for c-$Zr(8Y)O_2$. [§] These values of elastic modulus were calculated by rule of mixtures.

[†] In the rest of the paper, t-$Zr(3Y)O_2$ and c-$Zr(8Y)O_2$ will both be referred to as $Zr(Y)O_2$ whenever it is more convenient.

III. Results

(1) Thermal Expansion and K_c Values

The CTE's, measured courtesy of Harrop Inc., are shown in Fig. 2; data measured courtesy of Rockwell Science Center are reported in Table I along with calculated CTE values. The two sets of experimental data agree with one another and with the theoretical values. The CTE for the various compositions and the K_{Ic} values for *t*-Zr(3Y)O_2 and *c*-Zr(8Y)O_2 are listed in Table II along with other relevant material properties.

(2) Tunnel Crack Observations

Two types of cracks were observed in the Zr(Y)O_2 layers, i.e., cracks with a large opening displacement (≥30 μm) shown in Fig. 3(a) and cracks with a small opening displacement (≤2 μm) shown in Fig. 4(a). Three observations suggested that the cracks with a large opening displacement were caused by differential shrinkage before densification. First, the large crack opening could be caused only by the differential shrinkage strain associated with the differential particle packing of the materials that formed the two different layers. The relative density of the alumina/zirconia compositions, which varied from 0.56 (high Al_2O_3 content) to 0.47, was much higher than that of pure zirconia (≈0.40). Thus, the zirconia layers would shrink more than the adjacent alumina/zirconia layers during densification. Second, the surface of the crack with the large opening displacement showed smooth, round grains, identical to that of a free surface of the densified body as shown in Fig. 3(b). Third, Fig. 3(c) shows that the ends of the crack partially resintered where it penetrated into the adjacent Al_2O_3/Zr(Y)O_2 layer. Based on this evidence, it was concluded that the cracks with the large opening displacement were more likely formed during drying and that their large opening displacement was produced by differential shrinkage during densification. (Most of the cracks with the large opening displacement were observed during initial experiments, before a systematic method was developed to dry the specimens for densification.)

The surface of tunnel cracks with small opening displacements was exposed by fracturing diamond cut beams that included the tunnel crack. These surfaces (Fig. 4(b)) were identical to surfaces that were known to be produced by fracture. Figure 4(c) shows the fracture surface of a tunnel crack that extended into the adjacent Al_2O_3/Zr(Y)O_2 layer. In general, at least two crack front positions could be observed associated with the tunnel crack as shown in Fig. 4(c). This observation showed that the tunnel crack extended at least twice during cooling. The first position was likely produced when a critical

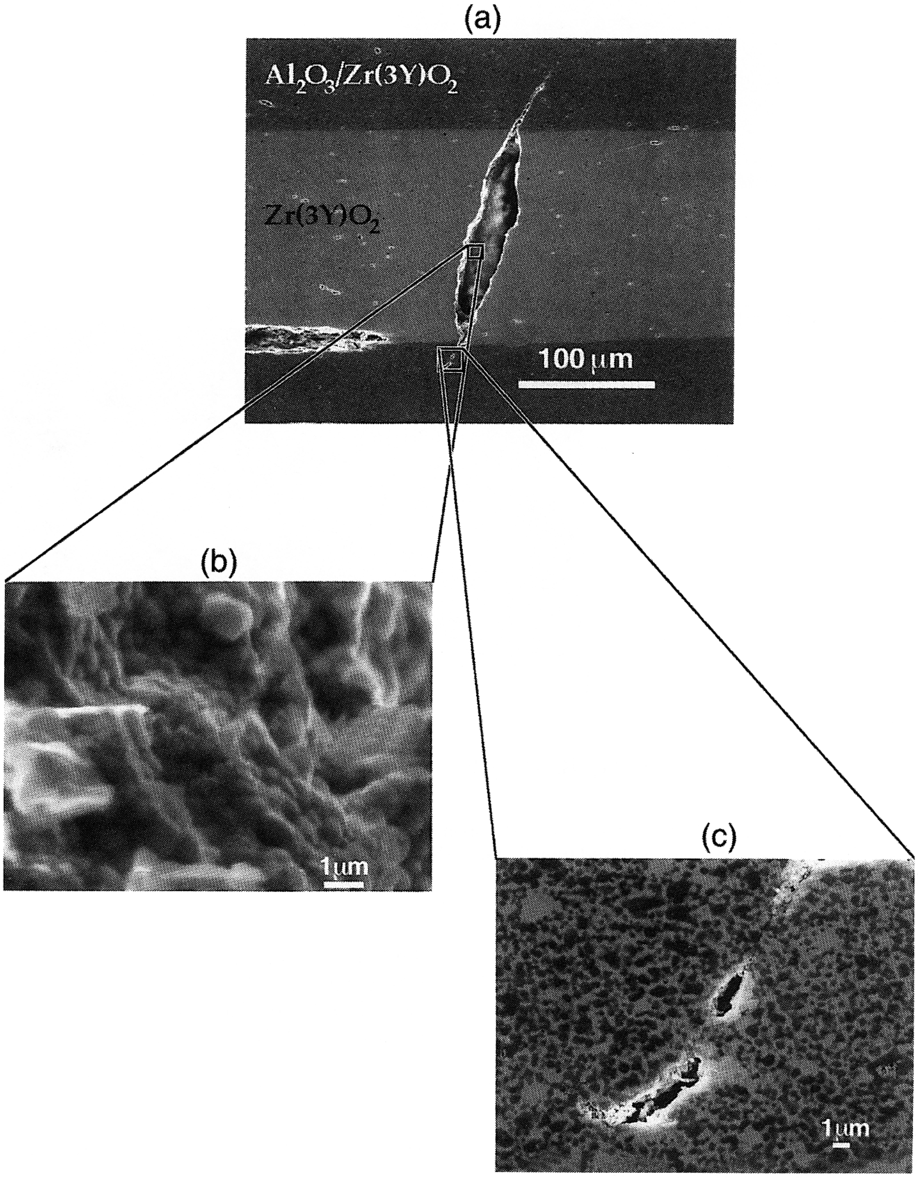

Fig. 3. (a) SEM micrograph of an open tunnel crack in an embedded layer of Zr(Y)O_2. (b) The crack surface of the open tunnel crack, composed of smooth, round grains. (c) Crack healing of the crack extension into the bulk material of Al_2O_3/Zr(Y)O_2.

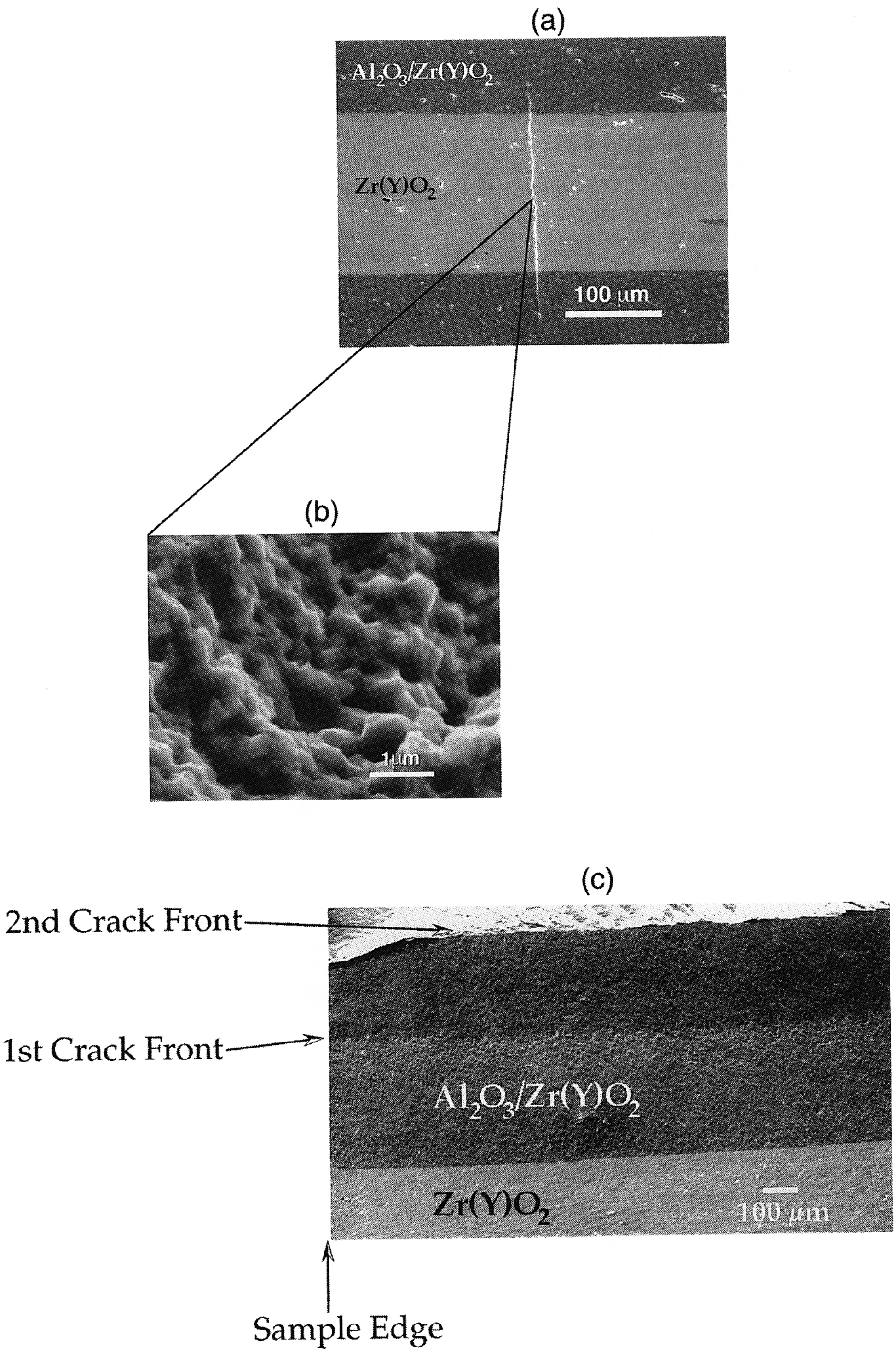

Fig. 4. (a) SEM micrograph of a closed tunnel crack in an embedded layer of $Zr(Y)O_2$. (b) The crack surface of the closed tunnel crack, composed of heavily faceted grains. (c) The fracture surface of a closed tunnel crack, showing two distinct crack front positions during crack extension into the adjacent $Al_2O_3/Zr(Y)O_2$ layer.

flaw in the tensile layer extended into the adjacent layers and then rapidly grew to a tunnel. Upon additional cooling, the tunnel extended farther in the adjacent layers. The second position in Fig. 4(c) was produced when the beam was fractured to reveal the surface of the tunnel crack. Only cracks with the small opening displacement, produced during cooling, will be of continued concern here.

Figure 5 shows the thickness of the $Zr(Y)O_2$ layer above which tunnel cracks were observed, for both the tetragonal and cubic layers, as a function of the composition of the adjacent $Al_2O_3/Zr(Y)O_2$ layers. The extension of the tunnel crack into the adjacent $Al_2O_3/Zr(Y)O_2$ layers, for laminates containing the $0.5Al_2O_3/0.5Zr(Y)O_2$ layers, is shown in Fig. 6 as a/t vs t, where a is the full length of the crack, including the portion that extends into the adjacent $Al_2O_3/Zr(Y)O_2$ layers, and t is the thickness of the $Zr(Y)O_2$ layer.

IV. Discussion

(1) Crack Penetration and Tunneling Analysis

The previous fracture mechanics analysis of tunnel cracking[14] did not consider crack extension into the adjacent layers, which is observed here and is obvious in hindsight. The analysis

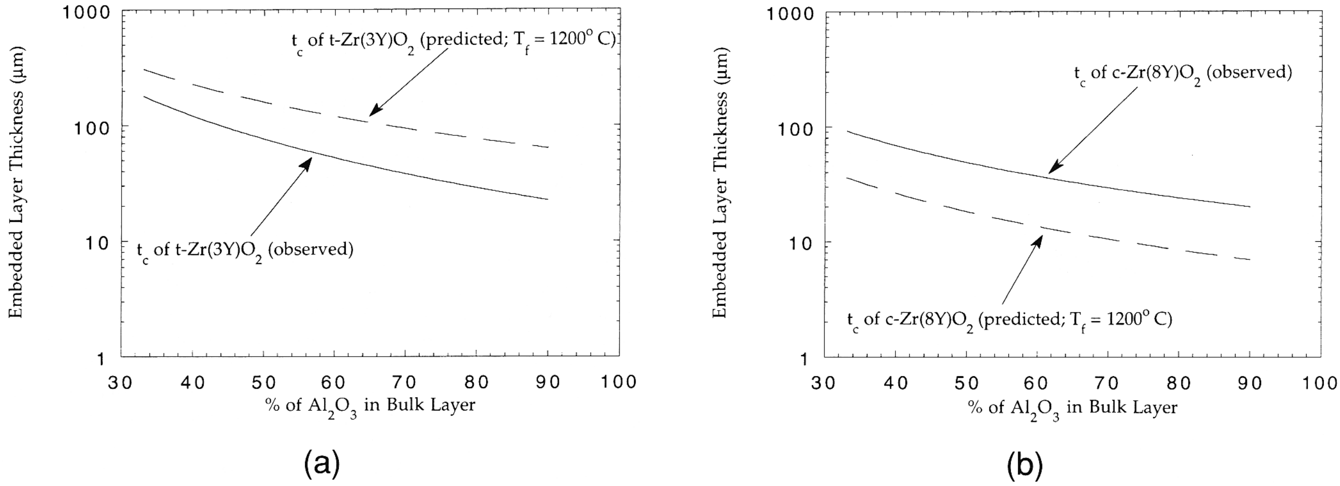

Fig. 5. (a) Plot of the critical layer thickness (t_c) observed in *t*-Zr(3Y)O_2 versus predicted critical layer thickness for varying percentage of Al_2O_3 in the adjacent layer (the greater the percentage of Al_2O_3 in the adjacent layer, the greater the residual stress in the embedded *t*-Zr(3Y)O_2 layer). (b) Plot of the critical layer thickness (t_c) observed in *c*-Zr(8Y)O_2 versus predicted critical layer thickness for varying percentage of Al_2O_3 in the adjacent layer.

that combines this extension into the adjacent layers with the tunneling phenomena will be described in the following paragraphs.

Consider a crack of length a in a layer of thickness t constrained by much thicker layers. For the moment, we will consider that both materials have identical elastic properties and identical fracture energy, G_c. We assume that the crack can extend across the interface into the adjacent, thicker layers and continue its extension as a tunnel crack, i.e., a crack that extends in the layer. The wake of the tunnel can be described as a slit crack. The strain energy release rate function for a slit crack within a layer subjected to tension and bounded by adjacent layers that contain no stress is given in Tada *et al.*[24] by

$$G_s = \left(\frac{\pi}{2}\right)\frac{\sigma^2}{E_1^*}\left(\frac{a}{t}\right)t \qquad a < t \qquad (5a)$$

$$G_s = \left(\frac{2}{\pi}\right)\frac{\sigma^2}{E_1^*}\left(\frac{a}{t}\right)\left[\sin^{-1}\left(\frac{t}{a}\right)\right]^2 t \qquad a > t \qquad (5b)$$

where $E_1^* = E_1/(1 - \nu_1^2)$, E_1 and ν_1 being the Young's modulus and Poisson's ratio of the tensile layer. A similar analysis was recently done by Watkins and Green,[25] in which they determined the condition for crack extension from a thin film into a thick substrate, when placing the whole system under applied tension (the effect of residual stresses was also taken into consideration). Figure 7 plots G_s normalized by $\sigma^2 t/E_1^*$ as a function of the normalized crack length, a/t. As the slit length a increases, the energy release rate increases when the slit is within the tensile layer, $a/t < 1$, and sharply decays when the slit extends into the adjacent layers, $a/t > 1$. Note that this energy release rate drives the slit to extend under the plane strain conditions. The trends of the curve, however, apply to an initial flaw of an arbitrary shape.

As previously detailed, the energy release rate that drives the crack to extend along the layer (tunneling) is given by[14,26]

$$G_t = \frac{1}{a}\int_0^a G_s(a)\,\mathrm{d}a \qquad (6)$$

A dimensional analysis shows that

$$G_t = \frac{Z\sigma^2 t}{E_1^*} \qquad (7)$$

where $Z = \pi/4$ when the elastic properties of the two materials are identical and $a = t$. In general, Z is a dimensionless driving force dependent upon elastic mismatch, crack geometry, and loading conditions.[26] The integral (6) is evaluated numerically and the result is plotted in Fig. 7. The tunneling energy release rate, G_t, is small for tunnels of both a very small and a very large width, a, and reaches the maximum value for a tunnel slightly extended into the adjacent layers. This maximum point coincides with the intersection point of the G_s and G_t curves. Note that the maximum value for Z is slightly above $\pi/4$.

Knowing the fracture energy G_c, the elastic modulus E^*, the tensile stress in the layer σ, and the layer thickness t, we can use Fig. 7 as a "map" to determine the conditions for crack extension and crack tunneling. The value of the normalized fracture energy, $(G_c E_1^*)/(\sigma^2 t)$, is represented by a horizontal line in Fig. 7, moving down during cooling due to an increase in the residual stress. As G_c moves into the hatched areas, either crack extension (below G_s) or crack tunneling (below G_t) can proceed. The hatched area under G_s in Fig. 7 contains two different regions, marked by the point at which the driving force for tunneling, G_t, is equal to the driving force for crack extension, G_s. The horizontal line contacting the G_t curve at its maximum intersects the G_s curve at another point, $(a/t)_0$. If the initial flaw in the tensile layer is larger than $(a/t)_0$, the crack will extend into the adjacent layers when $G_c = G_s$. At this point, $G_c > G_t$, so that a finite amount of further cooling (a lower G_c line) is necessary for the crack to tunnel. If the initial flaw is smaller than $(a/t)_0$, the crack propagates into the adjacent layers and tunnels at the same temperature.

We can also use Fig. 7 to interpret crack extension for the case where the laminar material contains tensile layers of different thicknesses that has been cooled to room temperature, thus fixing the tensile stress. The flaw cannot tunnel, regardless of its initial size and shape, if the horizontal line of the normalized fracture energy, $(G_c E_1^*)/(\sigma^2 t)$, is above the maximum point on the G_t curve. Rearranging Eq. (7), we obtain a critical thickness

$$t_c = \left(\frac{4}{\pi}\right)\frac{G_c E_1^*}{\sigma^2} \qquad (8)$$

(the approximate value $Z = \pi/4$ is used), below which no crack tunneling will occur, regardless of initial flaw size, a. Note, this is a conservative solution. When $t \geq t_c$ the probability of tunneling will still depend on the size of the flaw that preexists within the tensile layer.

The above analysis assumes identical elastic properties and identical fracture energy for both materials. If the fracture energies differ for the two materials, denoted as G_{c1} and G_{c2}, the crack extension in the adjacent layers is resisted by G_{c2}, and the tunneling is resisted by a combination of G_{c1} and G_{c2}. An analysis for thin film cracking is given in Ref. 27, which shows a moderate effect on the tunneling condition.

When the adjacent layers are more compliant than the tensile layer (smaller elastic modulus), the normalized energy release rate increases and the slit crack will extend a greater distance into the adjacent layers. The opposite conditions occur when

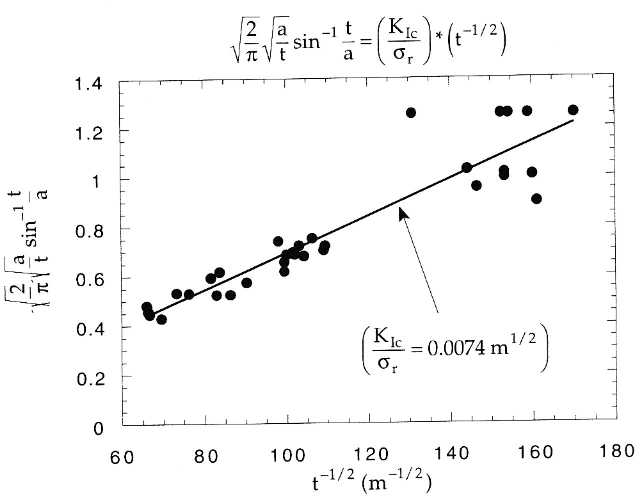

Fig. 6. Plot of crack length a versus embedded layer thickness t. This plot is arranged based upon Eq. (6). The slope of the plot is linear and is equal to K_{Ic}/σ_r.

the tensile layer is more compliant than the adjacent material. This is similar to the behavior seen in thin film cracking,[27] where a compliant substrate will "attract" a crack more than a stiff substrate. An interesting anomaly develops when the adjacent layer is much stiffer than the embedded layer. As seen in Fig. 8, the G function for the slit crack approaches zero on both sides of the interface. That is, the very stiff material blocks extension of the slit crack beyond the embedded layer. The effect is real, but if either the residual stress or the layer thickness is large enough, this "energy barrier" can be overcome, and the slit crack will extend into the bulk material.

(2) Comparison of Experiments with Analysis

Using the material parameters given in Table II, a predicted residual strain was calculated from Eq. (1). The initial temperature, T_i, used to determine the residual strain, was assumed to be 1200°C instead of the sintering temperature of 1500°C. This assumption was made because previous studies[28,29] have shown that zirconia exhibits significant plasticity above 1200°C. Therefore, we postulate that the $Zr(Y)O_2$ layers were sufficiently plastic to maintain a zero stress state above 1200°C. The temperature where the preexisting flaws start to extend during cooling is unknown; the room temperature was selected as the final temperature, T_f. While tunnel cracking may occur at higher temperatures, the analysis suggests that crack will continue to penetrate the adjacent layer during cooling. Predicted values of residual stress were determined by substituting the results from Eq. (1) into Eq. (3). The results from Eq. (3) for various compositions of $Al_2O_3/Zr(Y)O_2$ were then inserted into Eq. (8) to determine the critical layer thicknesses. The effect of the elastic mismatch between the embedded layers of $Zr(Y)O_2$ and the bulk material was considered. However, based on finite element analysis by Ho and Suo,[14] the value of Z, the driving force for crack propagation, does not change appreciably over the experimental range of the Dundurs Parameter, α_D ($-0.3 < \alpha_D < -0.1$). The effect of residual stress in the bulk materials was also considered. However, the maximum bulk residual stress in the laminates, which was ~50 MPa, was considered negligible. The values of the predicted critical thickness for various compositions are compared to the observed critical thicknesses for embedded layers of t-$Zr(3Y)O_2$ and c-$Zr(8Y)O_2$ in Figs. 5(a) and (b), respectively.

In Figure 5(a), the predicted values of the critical thickness are in reasonable agreement with the observed critical thicknesses, i.e., agreement within a factor of 2 to 3. The predicted critical thickness is not a conservative solution: the predicted values are *larger* than the experimental results. This is because the tunnel cracks apparently propagate at higher temperatures than assumed in the analysis. The fracture toughness of t-$Zr(3Y)O_2$ decreases with increasing temperature.[30] ‡ Therefore, the fracture toughness of the t-$Zr(3Y)O_2$ layer during tunneling is lower than the value measured at room temperature. Using the room-temperature value for fracture toughness for t-$Zr(3Y)O_2$ overestimates the critical thickness for crack extension.

Figure 5(b) shows the results of c-$Zr(8Y)O_2$, which is not transformation-toughened and therefore its fracture toughness is not expected to be as temperature-dependent as the tetragonal

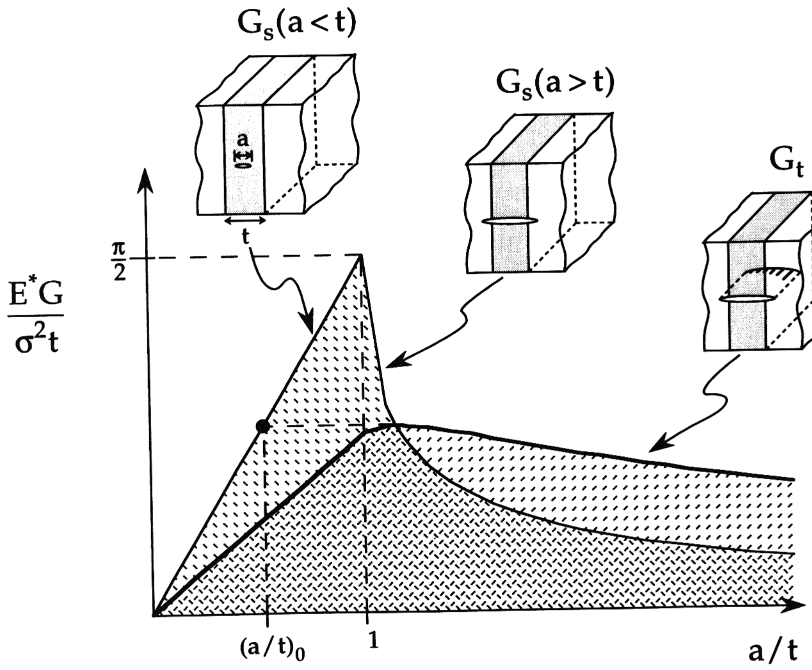

Fig. 7. Plot of the normalized strain energy release rate for crack extension (G_s) and crack tunneling (C_t) versus normalized crack length (a/t). When (a/t) is greater than $(a/t)_0$, crack extension occurs without tunneling. A finite amount of cooling is required to initiate crack tunneling. When (a/t) is less than $(a/t)_0$, crack extension occurs with tunneling.

---

‡ This is due to a lower driving force for transformation.

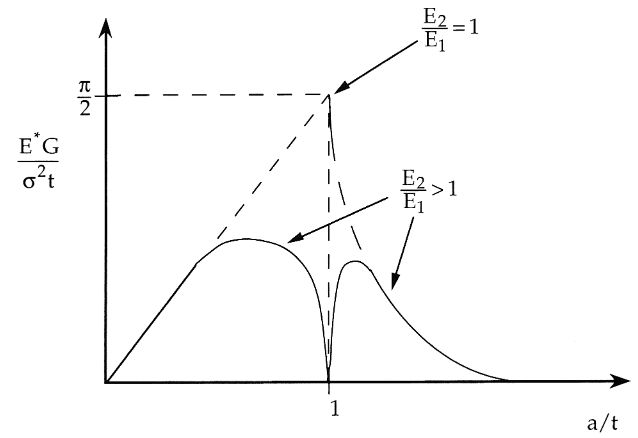

Fig. 8. (a) The change in the normalized energy release rate of a flaw, G, in an embedded layer with increasing crack length, a, when $E_2/E_1 = 1$ and when $E_2/E_1 > 1$. As the crack approaches the interface ($a/t = 1$), the normalized G_s reduces to 0, creating an "energy barrier," which can be overcome when the residual stress or the embedded layer thickness is large.

phase. As shown, the observed critical layer thickness is in good agreement with predicted values, because the predicted values maintain a conservative solution (no tunnel cracks were observed below the predicted critical layer thickness) and the experimental observations are within a factor of 2 of the theoretical predictions.

Experimental observations of crack extension into 0.50/0.50–Al_2O_3/t-Zr(3Y)O_2 layer is shown in Fig. 6 and compared to theoretical predictions. On the basis of Eq. (6) and the relation $G = K^2/E^*$ (K being the stress intensity factor), the slope of the plot should be constant and equal to K_{Ic}/σ. Figure 6 shows that the slope is linear. Substituting the value of σ in the tensile layer of 567 MPa, the fracture toughness, K_{Ic}, of the 0.50/0.50–Al_2O_3/t-Zr(3Y)O_2 layer was calculated to be 4.20 MPa·m$^{1/2}$, which is smaller by ≈25% than previously reported values.[29,30] This discrepancy is most likely due to crack extension occurring at temperatures higher than room temperature. Therefore, as stated for crack tunneling, the K_{Ic} measured for Al_2O_3/t-Zr(3Y)O_2 overestimates the toughness resisting crack extension.

V. Conclusion

An existing analysis for the extension of cracks in a layer under biaxial, residual tension is reported to take into account of crack penetration into the adjacent layers. Theoretical predictions of the critical layer thickness for tunnel cracks were then compared to experimental observations and were found to be in reasonable agreement and useful as a conservative solution in fabricating crack-free laminates. Experimental measurements of crack extension into the adjacent layers were found to be in good agreement with the analysis of a slit-crack.

Acknowledgments: The authors would like to thank Alex Blum of Harrop Industries, Dr. Wolfgang Pompe of the Max-Planck Institute in Dresden, and Dr. David Marshall of the Rockwell Science Center for measuring the coefficient of thermal expansion. The authors would also like to express their gratitude toward Mark Cornish for his assistance in electron microscopy and sample preparation.

References

[1] G. Behrens and A. H. Heuer, "Microstructural Characterization of Cofired Tungsten-Metallized High-Alumina Electronic Substrates," *J. Am. Ceram. Soc.*, **75** [10] 2815–24 (1992).

[2] S. Bruno, D. Swanson, and I. Burn, "High-Performance Multilayer Capacitor Dielectrics from Chemically Prepared Powders," *J. Am. Ceram. Soc.*, **76** [5] 1233–41 (1993).

[3] S. Iwanaga, T. Fujita, R. Iwamura, H. Yokono, S. Ueno, and S. Suzuki, "Fabrication Process of Air–Fuel Ratio Sensor by Using the Green-Sheet Laminating Materials"; pp. 49–68 in Advances in Ceramics, Vol. 19, *Multilayer Ceramic Devices.* Edited by J. Blum and W. R. Cannon. American Ceramic Society, Westerville, OH, 1987.

[4] T. Chartier, J. L. Besson, and P. Boch, "Mechanical Properties of ZrO_2-Al_2O_3 Laminated Composites"; pp. 1131–38 in Advances in Ceramics, Vol. 24B, *Science and Technology of Zirconia III.* Edited by S. Somiya, N. Yamamoto, and H. Yanagida. American Ceramic Society, Westerville, OH, 1988.

[5] J. Requena, R. Moreno, and J. S. Moya, "Alumina and Alumina/Zirconia Multilayer Composites Obtained by Slip Casting," *J. Am. Ceram. Soc.*, **72** [8] 1511–13 (1989).

[6] D. B. Marshall, J. J. Ratto, and F. F. Lange, "Enhanced Fracture Toughness in Layered Microcomposites of Ce-ZrO_2 and Al_2O_3," *J. Am. Ceram. Soc.*, **74** [12] 2979–87 (1991).

[7] P. Sarkar, X. Huang, and P. S. Nicholson, "Structural Ceramic Microlaminates by Electrophoretic Deposition," *J. Am. Ceram. Soc.*, **75** [10] 2907–909 (1992).

[8] C. J. Russo, M. P. Harmer, H. M. Chan, and G. A. Miller, "Design of a Laminated Ceramic Composite for Improved Strength and Toughness," *J. Am. Ceram. Soc.*, **75** [12] 3396–400 (1992).

[9] W. Cutler, F. Zok, and F. F. Lange, "Processing and Mechanical Properties of High Temperature Hybrid Multilayer Composites," in preparation.

[10] (a) H. Kirchner, J. Conway, and A. E. Segall, "Effect of Joint Thickness and Residual Stresses on the Properties of Ceramic Adhesive Joints: I, Finite Element Analysis of Stresses in Joints," *J. Am. Ceram. Soc.*, **70** [2] 104–109 (1987). (b) W. Zdaniewski, J. Conway, and H. Kirchner, "Effect of Joint Thickness and Residual Stresses on the Properties of Ceramic Adhesive Joints: II, Experimental Results," *J. Am. Ceram. Soc.*, **70** [2] 110–18 (1987).

[11] S. Johnson and D. Rowcliffe, "Mechanical Properties of Joined Silicon Nitride," *J. Am. Ceram. Soc.*, **68** [9] 468–72 (1985).

[12] A. Levy, "Thermal Residual Stresses in Ceramic-to-Metal Brazed Joints," *J. Am. Ceram. Soc.*, **74** [9] 2141–47 (1991).

[13] T. Garino and H. Bowen, "Deposition and Sintering of Particle Films on a Rigid Substrate," *J. Am. Ceram. Soc.*, **70** [11] C-315–C-317 (1987).

[14] S. Ho and Z. Suo, "Tunneling Cracks in Constrained Layers," *J. Appl. Mech.*, **60** [12] 890–94 (1993).

[15] M. S. Hu and A. G. Evans, "The Cracking and Decohesion of Thin Films on Ductile Substrates," *Acta Metall.*, **37** [3] 917–25 (1989).

[16] S. Ho, C. Hillman, F. F. Lange, and Z. Suo, "Surface Cracking in Layers under Biaxial, Residual Compressive Stress," *J. Am. Ceram. Soc.*, in press.

[17] J. C. Chang, F. F. Lange, and D. S. Pearson, "Viscosity and Yield Stress of Alumina Slurries Containing Large Concentrations of Electrolyte," *J. Am. Ceram. Soc.*, **77** [1] 19–26 (1994).

[18] B. V. Velamakanni, J. C. Chang, F. F. Lange, and D. S. Pearson, "New Method for Efficient Colloidal Particle Packing via Modulation of Repulsive Lubricating Hydration Forces," *Langmuir*, **6**, 1323–25 (1990).

[19] J. C. Chang, F. F. Lange, D. S. Pearson, and J. P. Pollinger, "Pressure Sensitivity for Particle Packing of Aqueous Al_2O_3 Slurries vs Interparticle Potential," *J. Am. Ceram. Soc.*, **77** [5] 1357–60 (1994).

[20] J. C. Chang, B. V. Velamakanni, F. F. Lange, and D. S. Pearson, "Centrifugal Consolidation of Al_2O_3 and Al_2O_3/ZrO_2 Composite Slurries vs Interparticle Potentials: Particle Packing and Mass Segregation," *J. Am. Ceram. Soc.*, **74** [9] 2201–204 (1991).

[21] W. Kreher and W. Pompe, *Physical Research: Internal Stresses in Heterogeneous Solids*, Vol. 9. Akademie-Verlag. Berlin, Germany, 1989.

[22] T. Nose and T. Fujii, "Evaluation of Fracture Toughness for Ceramic Materials by a Single-Edge-Precracked-Beam Method," *J. Am. Ceram. Soc.*, **71** [5] 328–33 (1988).

[23] J. E. Srawley, "Wide Range Stress Intensity Factor Expressions for ASTM E399 Standard Fracture Toughness Specimens," *Int. J. Fract.*, **12**, 475–76 (1976).

[24] H. Tada, P. C. Paris, and G. R. Irwin, *The Stress Analysis of Cracks Handbook*, 2nd Ed. Del Research, St. Louis, MO, 1985.

[25] T. R. Watkins and D. J. Green, "Fracture Behavior of CVD SiC-Coated Graphite: II, Conditions for the Onset of Multiple Cracking," *J. Am. Ceram. Soc.*, **77** [3] 717–20 (1994).

[26] J. W. Hutchinson and Z. Suo, "Mixed Mode Cracking in Layered Materials"; in *Advances in Applied Mechanics*, Vol. 29. Edited by J. W. Hutchinson and T. Y. Wu. Academic Press, New York, 1991.

[27] T. Ye, Z. Zuo, and A. G. Evans, "Thin Film Cracking and the Roles of Substrate and Interface, *Int. J. Solids Struct.*, **29** [21] 2639–48 (1992).

[28] T. Nieh and J. Wadsworth, "Superplastic Behaviour of a Fine-Grained, Yttria-Stabilized, Tetragonal Zirconia Polycrystal (Y-TZP)," *Acta Metall. Mater.*, **38** [6] 1121–33 (1990).

[29] D. S. Cheong, A. Dominguez-Rodriguez, and A. H. Heuer, "High-Temperature Plastic Deformation of Y_2O_3-Stabilized ZrO_2 Single Crystals: III. Variation in Work Hardening between 1200 and 1500°C," *Philos. Mag. A*, **63** [3] 377–88 (1991).

[30] F. F. Lange, "Transformation Toughening, Part 4: Fabrication, Fracture Toughness and Strength of Al_2O_3-ZrO_2 Composites," *J. Mater. Sci.*, **17**, 247–54 (1982).

[31] E. Bischoff and M. Ruhle, "Microcrack and Transformation Toughening of Zirconia-Containing Alumina"; see Ref. 4, pp. 635–43.

[32] K. Tsukuma, T. Takahata, and M. Shiomi, "Strength and Fracture Toughness of Y-TZP, Ce-TZP, Y-TZP/Al_2O_3, and Ce-TZP/Al_2O_3"; see Ref. 4, pp 721–28.

[33] Y. S. Touloukian, ed., *Thermophysical Properties of Matter: Thermal Expansion of Nonmetallic Solids*, Vol. 13. Plenum Publishing, New York, 1977.

[34] Dr. Dieter Schneider, private communication.

[35] R. L. Lehman, "Overview of Ceramic Design and Process Engineering"; p. 30 in *Engineered Materials Handbook: Ceramics and Glasses*, Vol. 4. ASM International, Materials Park, OH, 1991.

[36] B. Eigenmann, B. Scholtes, and E. Macherauch, "Roentgenologic Stress Determination in Ceramics and Metal–Ceramic Composites, Theory and Applications," *Materialwiss Werksfofftech.*, **20**, 314–25 (1989).

[37] K. Wefers and C. Misra, *Oxides and Hydroxides of Aluminum.* Alcoa Laboratories, Pittsburgh, PA, 1987.